Manipulation of the Lande g-factor in InAs quantum dots through application of anisotropic gate potentials

Sanjay Prabhakar[1,2], James E Raynolds[2] and Roderick Melnik[1,3]
[1] *M^2NeT Laboratory, Wilfrid Laurier University, Waterloo, ON, N2L 3C5 Canada*
[2] *College of Nanoscale Science and Engineering, State University of New York at Albany, 12203, USA*
[3] *BCAM, Bizkaia Technology Park, 48160 Derio, Spain*

(Dated: November 10, 2010)

We study the variation in the Lande g-factor of electron spins induced by an anisotropic gate potential in InAs quantum dots for potential use as non-charge based logic devices. In this paper, we present the numerical simulations of such spins in an electrostatically confined two-dimensional asymmetric gate potential forming a quantum dot system in a 2DEG. Using numerical techniques, we show that the broken in-plane rotational symmetry, due to Rashba spin orbit coupling in an asymmetric potential (induced by gate voltages) leads to a significant reverse effect on the tunability of the electron g-factor over a symmetric model potential (i.e. the derivative of the g-factor with respect to electric field has opposite sign in the two cases).

I. INTRODUCTION

The notion of manipulating single electron spins through active modification of the spin orbit interaction in a quantum dot formed in the plane of a two dimensional electron gas (2DEG) has received considerable attention for potential use in non charge-based logic devices and solid state quantum computing.[1–7] Such research is of interest in that it might enhance the possibilities of next generation spintronic logic devices based on CMOS technology.[8–15]

The goal of the present work is to explore the fundamental physics of a single electron spin trapped in an electrostatically defined quantum dot and to provide realistic information for controlling the Lande g-factor through the application of gate potentials. With an aim toward the practical design of such devices, we utilize a finite-element based numerical technique as was done in similar recently published work.[16] A key new result of the present work is the discovery that broken in-plane rotational symmetry due to the Rashba spin orbit coupling in an asymmetric potential, can lead to a significant reverse effect on the tunability of the electron g-factor over the symmetric case. We show that for a quantum dot with 30 nm radius the g-value increases (decreases) with increasing electric field if we apply symmetric (asymmetric) potentials ($\alpha = 1, \beta^2 = 80$).

The parameters of the asymmetric potential were chosen so as to mimic the realistic potential of a quantum dot in a single electron transistor that are under consideration by experimentalists at State University of New York at Albany. In particular, the geometry of the device and the methodology of obtaining the electrostatic potential along the symmetry axis and normal to the symmetry axis are described in Ref. 17. By choosing $\alpha = 1$, $\beta^2 = 2.8$ and the value of ω_o, most conveniently expressed equivalently by $\ell_o = \sqrt{\hbar/(m^\star\omega_0)} \approx 30$ nm in the asymmetric parabolic confining potentials $\frac{1}{2}m^\star\omega_0^2(\alpha^2x^2 + \beta^2y^2)$ in Eq. 2 reflects the realistic potential of the realistic device.[17]

The key parameters in controlling the electron spin in a single electron quantum dot, considered in this work, are the Rashba[18] and Dresselhaus[19] spin orbit couplings. These two spin orbit coupling effects arise from two different types of symmetry operations in III-V type semiconductors. The Rashba spin orbit coupling arises from the structural inversion asymmetry of the triangular shaped quantum well confining potential, while bulk inversion asymmetry (due to the Zincblene structure) gives rise to the Dresselhaus spin orbit coupling. The mathematical expressions for these interactions are given in Eqs. 4, 5, and 6, in the following, and are well established for semiconductor heterojunction-type devices.[9,11,15,20,21]

It is also generally understood that the Zeeman spin splitting energy depends on the direction of an applied magnetic field and is thus described by a g-factor *tensor*.[13,22–24] In the present work we only consider magnetic fields normal to the 2DEG, so the g-factor tensor reduces to a scalar. In several recent works, anisotropy effects in coupled quantum dot systems were explored.[25–28] A subject that seems to have received little attention, however, is the question of anisotropic effects in single quantum dots (electrostatically defined in a 2DEG by asymmetric gate potentials) and it is the subject of the present investigation. Our approach is most closely related to that of Ref. 8 but differs in a sense that we take a numerical approach based on the finite element method[29] whereas the authors of Ref. 8 use the perturbation theory and direct diagonalization techniques and didn't consider anisotropy effects. Similar types of results have also been reported in Ref. 30. However, our methodology is different in a sense that we utilize the finite element method and study the g-factor in InAs quantum dots for realistic anisotropic gate potentials. The authors in Ref. 30 adopted an atomistic tight binding method and studied the effects of donors in the g-value vs electric and magnetic fields. We now turn to a discussion of our model, followed by a brief description of our computation methodology.

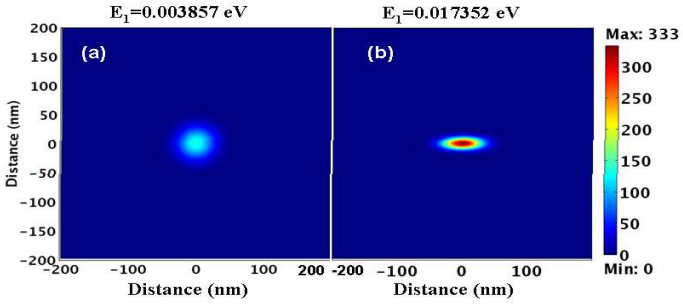

FIG. 1. (Color online) In plane wave functions for quantum dots formed by (a) symmetric quadratic potential with $\alpha = \beta = 1$, and (b) asymmetric quadratic potential with $\alpha^2 = 1, \beta^2 = 80$. In both cases, we choose $\ell_0 = 30$ nm, electric field $= 10^5$ v/cm, and magnetic field $= 1$ T.

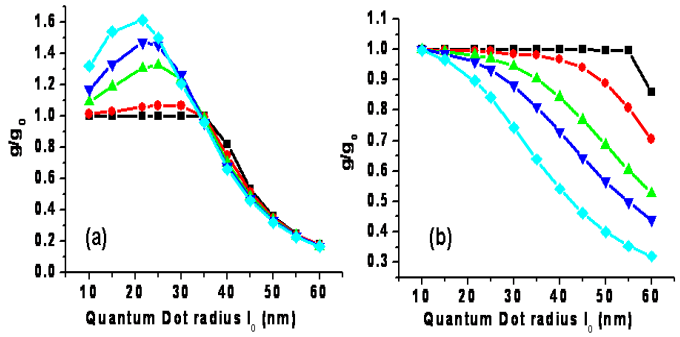

FIG. 2. (Color online) Electric-field induced changes in the g-factor vs quantum dot radius for symmetric and asymmetric model potentials with (a) $\alpha = \beta = 1$ and (b) $\alpha^2 = 1, \beta^2 = 80$. In Fig 2(a), from bottom to top, the curves represent increasing electric field strength as $1\times10^4, 2\times10^5, 5\times10^5, 7\times10^5$ and 10^6 v/cm. In Fig 2(b), from top to bottom, the curves represent increasing electric field strength as $1 \times 10^4, 2 \times 10^5, 5 \times 10^5, 7\times10^5$ and 10^6 v/cm. In both cases, We choose the magnetic field $= 1$ T. We express g relative to its nonrelativistic free electron value $g_0 = 2$. We find a level crossing near 35 nm quantum dot radius in Fig 2(a) and 55 nm quantum dot radius in Fig 2(b).

II. THEORETICAL MODEL

We consider the motion of the electron in the $x - y$ plane of the quantum dot in the presence of a magnetic field oriented along z-direction. Our approach closely follows that of Ref. 8 and 17. Thus the total Hamiltonian can be written as:

$$H = H_{xy} + H_z + H_{so}, \tag{1}$$

where H_z corresponds to the motion of the electron in a quantum dot normal to the interface (as discussed in the Ref. 8), H_{so} is the spin-orbit interaction to be discussed shortly and the remaining term is given by:

$$H_{xy} = \frac{\vec{P}^2}{2m} + \frac{1}{2}m\omega_o^2(\alpha^2x^2 + \beta^2y^2) + \frac{1}{2}g_o\mu_B\sigma_zB, \tag{2}$$

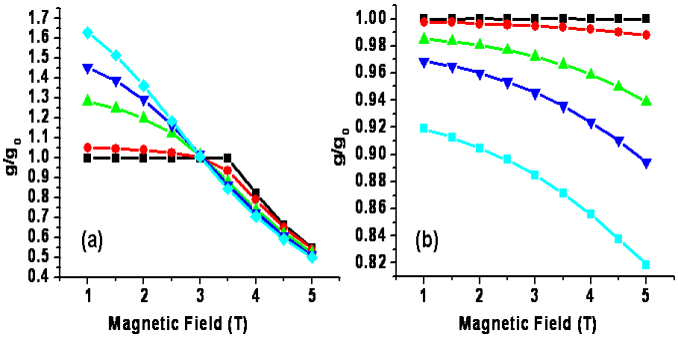

FIG. 3. (Color online) Electric-field induced changes in the g-factor vs magnetic field for symmetric and asymmetric model potentials with (a) $\alpha = \beta = 1$ and (b) $\alpha^2 = 1, \beta^2 = 80$. In Fig. 3(a), from bottom to top, the curves represent increasing electric field strength as $1\times10^4, 2\times10^5, 5\times10^5, 7\times10^5$ and 10^6 v/cm. In Fig. 3(b), from top to bottom, the curves represent increasing electric field strength as $1\times10^4, 2\times10^5, 5\times10^5, 7\times10^5$ and 10^6 v/cm. In both cases, we choose $\ell_0 = 20$ nm. We express g relative to its nonrelativistic free electron value $g_0 = 2$. We find a level crossing near 3 T in Fig 3(a) and its value extends to the larger magnetic field in Fig 2(b).

where the kinetic momentum operator: $\vec{P} \equiv \vec{p} + \frac{e}{c}\vec{A}$ is the sum of the canonical momentum: $\vec{p} \equiv -i\hbar(\partial_x, \partial_y, 0)$, and the vector potential (in the symmetric gauge) $\vec{A} \equiv \frac{B}{2}(-y, x, 0)$.

The eigenstates of H_{xy} in Eq. 2 with $\alpha = \beta$ are the well-known Fock-Darwin energy states.[31,32] The situation with $\alpha \neq \beta$ also has an analytic solution.[33,34] We have verified that our numerical solution of $H_{xy}|\psi> = \epsilon|\psi>$ is consistent with the analytical results of the Lande g-factor of the anisotropic case, obtained by using the perturbative method.

Lastly, we consider the Hamiltonian associated with Rashba and Dresselhaus spin orbit interactions that is embodied in the Hamiltonian H_{so}. These spin orbit interactions are the essential ingredient in the phenomena of switching electron spin with gate potentials.[5,8] We write:

$$H_{so} = H_R + H_{D1} + H_{D2}, \tag{3}$$

where the *Rashba* interaction[18,35] is given by:

$$H_R = \frac{\alpha_R eE}{\hbar}\Big(\sigma_xP_y - \sigma_yP_x\Big), \tag{4}$$

and the linear and cubic *Dresselhaus* interactions[19,36] are written as:

$$H_{D1} = \frac{0.7794\gamma_c k^2}{\hbar}\Big(-\sigma_xP_x + \sigma_yP_y\Big), \tag{5}$$

which is linear in components of the momentum operator $\vec{P}$ and

$$H_{D2} = \frac{\gamma_c}{\hbar^3}\Big(-\sigma_xP_xP_y^2 - \sigma_yP_yP_x^2\Big) + h.c., \tag{6}$$

which is cubic in components of the momentum operator. Here, *h.c.* denotes the Hermitian conjugate.[8] Note, the electric field strength E that enters Eq. 4 is associated with the heterojunction $|E| = \partial V(z)/\partial z$ along z-direction and is treated as an adjustable parameter. From a physical point of view, we can make changes in E through the application of appropriate gate potentials. All numerical parameters for InAs are taken from the Ref. 8

The eigenvalue equation $H\,|\,\psi> = \epsilon|\,\psi>$, with H given by Eqs. 1 through 6, was solved numerically to obtain the lowest few eigenvalues and eigenstates vs the various parameters of the system. These parameters include the magnetic field strength B, the electric field E, and the strength of the quantum dot confinement potential as specified by the quantum dot radius $\ell_o = \sqrt{\frac{\hbar}{m^\star \omega_0}}$.

The notion of electric field induced spin switching is quantified by defining an effective electron g factor by,

$$\epsilon = \frac{1}{2} g \mu_B \sigma_z B, \tag{7}$$

to describe the energy difference between the lowest energy up and down spin states. Thus, we consider the lowest two states (including spin) ϵ_2 and ϵ_1 and calculate the effective g factor as:

$$g = \frac{\epsilon_2 - \epsilon_1}{\mu_B B}. \tag{8}$$

Results for the variation of this effective g factor as a function of the parameters E, B and ℓ_o are presented in the following section.

III. RESULTS AND DISCUSSIONS

The main observation is: the in-plane symmetry breaking in an anisotropic potential (i.e. $\alpha \neq \beta$) gives rise to qualitatively different behavior for the tunability of the electron g-factor with the application of electric and magnetic fields as compared to a symmetric potential (i.e. $\alpha = \beta = 1$).

We focus our attention on motion in the plane of the 2DEG and contrast the effects associated with the quantum dots in symmetric and asymmetric confining potentials as illustrated in Figs. 1(a) and 1(b), respectively. These figures were obtained by using the quadratic model potentials with $\alpha = \beta = 1$ for the symmetric case as in Fig. 1(a) and $\alpha^2 = 1$ and $\beta^2 = 80$ for asymmetric case as in Fig. 1(b), in the Hamiltonian H_{xy}, describing motion in the plane of 2DEG (i.e., x-y plane). The quantum dot radius defined by $\ell_o = \sqrt{\frac{\hbar}{m^\star \omega_0}}$ was choosen to have the value $\ell_0 = 30$ nm. The in-plane symmetry breaking due to anisotropic gate potentials can be contrasted by comparing the wave function of the electron in symmetric and asymmetric model potentials in the plane of 2DEG as shown in Figs. 1(a) and 1(b).

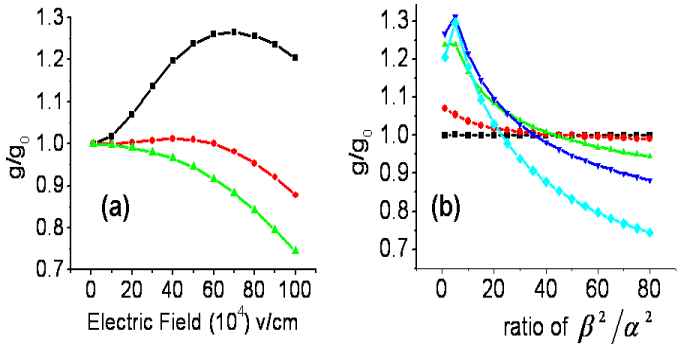

FIG. 4. (Color online) (a) Changes in the g-factor vs electric filed for quantum dots in the model potential characterized by $\alpha = 1, \beta = 1$ (black), $\alpha = 1, \beta^2 = 40$ (red)$\alpha = 1, \beta^2 = 80$ (green). (b) Electric field induced changes in the g factor vs the degree of anisotropy of the quantum dot confinement potential for various electric field strengths. In each plot, from bottom to to, the curves represent increasing electric field strength as $1\times10^4, 2\times10^5, 5\times10^5, 7\times10^5$ and 10^6 v/cm. We choose B=1 T and $\ell_0 = 30$ nm in each plot. We express g relative to its nonrelativistic free-electron value $g_0 = 2$.

Figure 2(a) is consistent with previously published work[8] and illustrates the g-factor tunability vs the strength of the applied electric field and confining potential (as parametrized by the quantum dot radius ℓ_o) for fixed magnetic field ($B = 1$ T) for the symmetric quantum dot in the quadratic potential of $\alpha = \beta = 1$. We express g relative to its non-relativistic free-electron value $g_o = 2$. We found that there is an abrupt change in the g-value vs quantum dot radius near 35 nm for the symmetric potential. This is due to level crossings (two eigenstates have the same spin) in the quantum dot system, as considered in Eq. 8.

Figure 3(a) is also consistent with previously published work[8] and illustrates the g-factor tunability vs the strength of the applied electric and magnetic fields for fixed confining potential (parametrized by the quantum dot radius $\ell_o = 20$ nm). Again, we found a level crossing near 3 T for the asymmetric potential.

To quantify the effects of in-plane anisotropy, we have carried out a parameter study of the g-factor tunability vs several variables in an anisotropic case such as quantum dot radius (ℓ_0) in Fig. 2, magnetic field (B) in Fig. 3, electric field in Fig. 4(a), and degree of anisotropy (β^2/α^2) in Fig. 4(b).

First, we consider the results for g-factor tunability for quantum dots in the asymmetric confining potential of Figs. 2(b) and 3(b). Figure 2 illustrates the tunability of the Lande g-factor vs electric field and confining potential ℓ_0 in the symmetric potential in comparison with the model potential with parameters $\alpha^2 = 1$ and $\beta^2 = 80$. The lowest curve in Fig. 2(a), indicated by filled black squares, represents the symmetric model potential of $\alpha = \beta = 1$ and the other curves with filled symbols represent varying electric fields of $(2, 5, 7, 100) \times 10^5$ v/cm. Similarly, the top curve in Fig. 2(b), indicated by filled

black squares, represents the asymmetric model potential of $\alpha^2 = 1, \beta^2 = 80$ and the other curves with filled symbols represent varying electric fields of $(2, 5, 7, 100) \times 10^5$ v/cm. In each case of the symmetric and asymmetric quadratic model potentials, we have chosen $B = 1$ T. By introducing the in-plane asymmetric potential, we found that the tunability of the electron g-factor is extended to larger quantum dot radius (roughly 55 nm quantum dot radius).

Figure 3 illustrates the tunability of the Lande g-factor vs magnetic field in the symmetric potential in comparison with the asymmetric potential characterized by parameters $\alpha^2 = 1$ and $\beta^2 = 80$. The lowest curve in Fig. 3(a), indicated by filled black squares, represents the symmetric model potential of $\alpha = \beta = 1$ and the other curves with filled symbols represent varying electric fields of $(2, 5, 7, 100) \times 10^5$ v/cm. Similarly, the lowest curve in Fig. 3(b), indicated by filled black squares represents the asymmetric model potential with $\beta^2/\alpha^2 = 80$ and the other curves with filled symbols represent varying electric fields of strength $(2, 5, 7, 100) \times 10^5$ v/cm. In each case (symmetric and asymmetric model potentials), we have chosen $\ell_0 = 20$ nm. Again, we found that the tunability of the electron g-factor increases with the larger magnetic field.

Figure 4(a) illustrates the g-factor tunability vs electric field and degree of anisotropy in both cases: symmetric and asymmetric model potentials. The top curve in Fig. 4(a), indicated by filled black squares, represents the symmetric model potential of $\alpha = \beta = 1$ and the other curves with filled symbols represent varying anisotropic potentials from $\beta^2/\alpha^2 = 40$ and $\beta^2/\alpha^2 = 80$. As before, we choose, $B = 1$ T and $\ell_0 = 30$ nm.

Lastly, Figure 4(b) illustrates the tunability of the g-factor to the degree of anisotropy in the model potential. The lowest curve in Fig. 4(a), indicated by filled black squares, represents the symmetric model potential of electric field $E = 10^4$ v/cm and the other curves with filled symbols represent varying electric fields $2 \times 10^5, 5 \times 10^5, 7 \times 10^5$ and 10^6 v/cm. We choose, $B = 1$ T and $\ell_0 = 30$ nm.

The g-factor tunability vs electric field for several degrees of anisotropic gate potentials in Fig. 4(a) has been compared to the results in Ref. 17. The authors in Ref. 17 claimed that there is a small variation in the g-factor with the variation of electric fields for $\beta^2/\alpha^2 = 1, 2.8, 5$ and 10 in a fixed confining potential of GaAs quantum dot radius, $\ell_0 = 30$ nm due to both Rashba and Dresselhaus spin orbit interactions. However, in Fig. 4(a), we can see that there is a reverse effect in the tunability of the Lande g-factor vs electric field for several degrees of anisotropic gate potentials. Broken in-pane rotational asymmetry in InAs quantum dots due to the Rashba spin orbit coupling for asymmetric confining potentials gives rise to the reverse effect over symmetric potentials.

The level crossing (two eigenstates have same spin) starts at larger quantum dot radius in an anisotropic confining potential compared to that of symmetric confining potential. It means that the anisotropy extends the tunability of the Lande g-factor to a larger quantum dot radius due to broken in-plane rotational asymmetry in InAs quantum dots. This causes a monotonous decrease in the Lande g-factor vs electric field in asymmetric confining potential ($\beta^2/\alpha^2 = 40(red), 80(green)$ over symmetric confining potentials ($\beta^2/\alpha^2 = 1(black)$ as shown in Fig. 4(a).

IV. CONCLUSIONS

We have carried out a numerical simulation study of gate induced tunability of the electron g-factor in a prototype single electron spintronic device. We have considered symmetric and asymmetric quadratic model potentials in the plane of 2DEG and employed a numerical approach based on the finite element method.

The key result of this work is illustrated in Figs. 2, 3 and 4: anisotropic potential induced by gate voltages in the plane of 2DEG breaks the in-plane rotational symmetry due to the Rashba effect.

Indeed, in Fig. 2(a) we see that all of the curves collapse onto a single curve for large quantum dots (i.e. starting around $\ell_o = 35$ nm) negating the switching effect. With anisotropy, however, the range of switchability is shifted to larger dots. In Fig. 2(a), the Lande g-factor increases from 0.98 to 1.2 at $\ell_0 = 30$ nm with the increase in the electric field for the symmetric potential ($i.e., \alpha = \beta = 1$). However, in Fig. 2(b), the Lande g-factor decreases from 0.98 to 0.82 at $\ell_0 = 30$ nm with the increase in the electric field for the asymmetric potential ($i.e., \beta^2/\alpha^2 = 80$). In Fig. 4(a), we see that the g-factor increases with the increase in electric field (filled black squares) for the symmetric potential. However, g-factor decreases with the increase in electric field in an anisotropic potential (filled red circles $\beta^2/\alpha^2 = 40$ and filled green triangles pointing down, $\beta^2/\alpha^2 = 80$).

Another result of this work is the variation in the Lande g-factor with respect to the magnetic field as well as electric field in both symmetric and asymmetric potentials for fixed quantum dot radius ℓ_0) that was illustrated in Fig. 3(a) and Fig. 3(b). Here, we quantify the Lande g-factor increases from 0.98 to 1.5 with the increase in electric field from 1×10^4 v/cm to 100×10^4 v/cm at the magnetic field of 2 T for the symmetric potential ($i.e., \alpha = \beta = 1$) as shown in Fig. 3(a). However, the Lande g-factor decreases from 0.98 to 0.90 with the increase in electric field from 1×10^4 v/cm to 100×10^4 v/cm at the magnetic field of 2 T for asymmetric potential ($i.e., \alpha \neq \beta$) as shown in Fig. 3(b).

Lastly, we see that the degree of anisotropy needs not to be very large in order to obtain significant changes in the gate induced g-factor tunability, as illustrated in Fig. 4(b). We see that the g-factor increases with the increase in the electric field for the anisotropic ratio of up to $\beta^2/\alpha^2 = 25$. Above this value, the g-factor starts decreasing with the increase in electric field. The

monotonous decrease in the Lande g-factor in asymmetric confining potential confirms that anisotropy extends the tunability of the Lande g-factor to a larger quantum dot radius due to the Rashba spin orbit coupling.

By employing a fully numerical approach, we have shown that breaking in-plane rotational symmetry in an asymmetric potential can lead to a significant change in the tunability of the electron g-factor over the symmetric model potential.

ACKNOWLEDGMENTS

The authors acknowledges Dr. Eduard Takhtamirov for his many helpful discussions. This work was supported by NSERC and CRC program, Canada.

[1] H.-A. Engel, L. P.Kouwenhoven, D. Loss and C. M. Marcus, Quantum Information Processing **3**, 115 (2004).
[2] W. A. Coish and D. Loss, Phys. Rev. B **75**, 161302 (2007).
[3] D. D. Awschalom, D. Loss and N. Samarth, Semiconductor Spintronics and Quantum Computation, Springer, Berlin (2002).
[4] R. Hanson, L. P. Kouwenhoven, J. R. Petta, S. Tarucha, L. M. K. Vandersypen, Rev. Mod. Phys. **79**, 1217 (2007).
[5] I. Žutić, J. Fabian and S. Das Sarma Rev. Mod. Phys. **76**, 323 (2004).
[6] S. Bandyopadhyay, Phys. Rev. B **61**, 13813 (2000).
[7] A. R. Trivedi and S. Bandyopadhyay, J. Appl. Phys. **103** 104311, (2008).
[8] R. de Sousa and S. Das Sarma, Phys. Rev. B **68**, 155330 (2003).
[9] E. I. Rashba and A. L. Efros, Appl. Phys. Lett. **83**, 5259 (2003).
[10] E. I. Rashba and A. L. Efros, Phys. Rev. Lett. **91**, 126405 (2003).
[11] E. A. Laird, C. Barthel, E. I. Rashba, C. M. Marcus, M. P. Hanson and A. C. Gossard, Phys. Rev. Lett. **99**, 246601 (2007).
[12] C. S. Tang, A. G. Mal'shukov and K. A. Chao, Phys. Rev. B **71**, 195314 (2005).
[13] J. Pingenot, C. E. Pryor and M. E. Flatté Appl. Phys. Lett. **92**, 222502 (2008)
[14] K. C. Nowack, F. H. L. Koppens, Y. V. Nazarov and L. M. K. Vandersypen, Science **318**, 1430 (2007).
[15] A. L. Efros, E. I. Rashba and M. Rosen, Phys. Rev. Lett. **87**, 206601 (2001).
[16] C. E. Pryor and M. E. Flatté, Phys. Rev. Lett. **96**, 026804 (2006).
[17] S. Prabhakar and J. E. Raynolds, Phys. Rev. B **79**, 195307 (2009).
[18] Y. A. Bychkov, and E. I. Rashba J. Phys. C: Solid State Phys. **17**, 6039 (1984).
[19] G. Dresselhaus, Phys. Rev., **100**, 580 (1955).
[20] L. S. Levitov and E. I. Rashba, Phys. Rev. B **67**, 115324 (2003).
[21] J.-M. Tang, J. Levy and M. E. Flatté, Phys. Rev. Lett. **97**, 106803 (2006).
[22] Y. Kato R. C. Myers A. C. Gossard J. Levy D. D. Awschalom, Science **299**, 1201 (2003).
[23] C. F. Destefani and S. E. Ulloa, Phys. Rev. B **71**, 161303 (2005).
[24] T. Andlauer and P. Vogl, Phys. Rev. B **79**, 045307 (2009).
[25] R. Ravishankar, P. Matagne, J. P. Leburton, R. M. Martin and S. Tarucha, Phys. Rev. B **69**, 035326 (2004).
[26] B. Szafran, F. M. Peeters and S. Bednarek, Phys. Rev. B **70**, 205318 (2004).
[27] I. L. Aleiner and V. I. Fal'ko, Phys. Rev. Lett. **87**, 256801 (2001).
[28] A. Kwasniowski and J. Adamowski, J. Phys. Cond. Matt. **20**, 215208 (2008).
[29] Comsol Multiphysics version 3.5a (www.comsol.com).
[30] R. Rahman, S. H. Park, T. B. Boykin, G. Klimeck, S. Rogge L. C. L. Hollenberg Phys. Rev. B **80**, 155301 (2009).
[31] V. Fock, Physik **47**, 446 (1928).
[32] C. G. Darwin, Proc. Cambridge Philos. Soc. **27**, 86 (1930).
[33] B. Schuh, J. Phys. A: Math. Gen. **18**, 803 (1985).
[34] S. Prabhakar, J. E. Raynolds and A. Inomata, SPIE proceedings **7702**, 77020V (2010).
[35] E. I. Rashba, Fiz. Tverd. Tela (Lenningrad) **2**, 1224 (1960).
[36] M. Dyakonov and V. Kachorovskii, Fiz. Tekh. Poluprovodn. (S.-Petersburg) **20**, 178 (1986).